Graphical Abstract

Location dependent flight cost differences from the moon and its influence on ISRU location selection for exporta

Sven J. Steinert, Paul Zabel, Dominik Quantius

Highlights

Location dependent flight cost differences from the moon and its influence on ISRU location selection for export

Sven J. Steinert, Paul Zabel, Dominik Quantius

- Research highlight 1

- Research highlight 2

Location dependent flight cost differences from the moon and its influence on ISRU location selection for export

Sven J. Steinert[a,*], Paul Zabel[b], Dominik Quantius[b]

[a]TU Munich, Boltzmannstr. 15, Garching, 85748, Bavaria, Germany
[b]German Aerospace Center (DLR), Institute of Space Systems, Robert-Hooke-Str. 7, Bremen, 28359, Bremen, Germany

Abstract

Keywords:

1. Overview

When a fully robotic ISRU production factory is feasible on the lunar surface, the location selection is not anymore bound to life support systems and the water resources they require. Therefore an optimization on the process factors can be applied to pick the most optimal location globally, instead being limited to polar regions only. For this event, this analysis is trying to identify the leading significance of the two sections of process factors, the ISRU efficiency (A) and the Transport efficiency (B), when an export aspect is considered. Hereby each section is inspected separately first before they are combined in a joined model (chapter 4) to compare the more relevant influence.

1.1. Scenario

In particular the ISRU production plant produces Oxygen as propellant component that is exported to an orbital propellant depot. The annual Oxygen production is 23.9 t (chapter 2.1) that is transported via a round trip of a rocket launch system (chapter 3.1) over [x] runs annually to the fuel-depot at target destination (chapter 3.2). The mission duration is designed over a period of 10 years.

2. Option A - ISRU efficiency

When the optimal location is chosen by the highest ISRU efficiency, the whole production line has to be inspected for location dependent factors first. Such location dependent factors are for example: raw material concentration, solar irradiance, temperatures, flat surface conditions and further scenic requirements. Hereby, the production method is decisive about the sensitivity to location dependend factors. Where hydrogen reduction of ilmenite features a high dependency on the raw material concentration, molten regolith electrolysis for example is mostly invariant to it over the lunar surface. In this paper hydrogen reduction of ilmenite is chosen as the production method to be analysed, which we expect to have a rather strong location dependency. All results that are derived here are therefore only applicable to this single production method.

2.1. Model

To simplify model complexity, our model does include only the raw material concentration factor as argument, the Ilmenite weight ratio. While not covering all influences, this factor we are assuming the most significant for location dependency and serves as our approximation to the full model of hydrogen reduction of ilmenite. The goal here is not to give a precise value but to get in the right order of magnitude for a comparison later. The model cost is defined as the hardware mass that has to be moved to the lunar surface for ISRU operation which is to be minimized. In a previous work of Francisco J. Guerrero-Gonzalez this hardware mass depending on Ilmenite concentration was determined for a combined production plant of Low Carbon Steel and Oxygen production. This production plant was sized for an annually output of 23.9 t Oxygen and 25 t Low Carbon Steel. The model consists out of a sum of required subsystems as defined in Equation 1 below.

$$
\begin{aligned}
y_0(x) &= 4036 \cdot x^{-1.064} - 9.59 && \text{Excavation}\\
y_1(x) &= 17580 \cdot x^{-1.003} - 390.8 && \text{Handling}\\
y_2(x) &= 19240 \cdot x^{-1.003} - 421.9 && \text{Beneficiation}\\
y_3(x) &= 21780 \cdot x^{-1.198} + 120.3 && \text{O2 Extraction}\\
y_4(x) &= 17910 \cdot x^{-1.265} + 1370 && \text{O2 Purification}\\
y_5(x) &= 29650 \cdot x^{-0.7005} - 602.5 && \text{Metal Processing}\\
y_6(x) &= 2541 \cdot x^{-0.7434} + 286.8 && \text{Gas Liquefaction \& Storage}\\
y_7(x) &= 32440 \cdot x^{-0.8312} + 125.2 && \text{Thermal Control}\\
y_8(x) &= 12000 \cdot x^{-0.9657} + 63.99 && \text{Power}
\end{aligned}
$$

$$
\mathrm{m}_{\mathrm{hardware}}(x = w_{\mathrm{ilmenite}}) = \sum_{i=0}^{8} y_i(x) \tag{1}
$$

*Corresponding author
Email address: sven.julius.steinert@outlook.com (Sven J. Steinert)

Where in our scenario only the Oxygen production is relevant, the additional subsystems as Metal Processing scale in a similar way as the rest of the system so that the spread between low and high values of x is not distorted significantly (88.69% spread to the maximum value vs. 89.97% spread without Metal Processing, with $1 \leq x \leq 11$). Furthermore this combined production plant could still be a viable choice out of the synergetic effects of shared infrastructure. This is why we are choosing this to be our reference production plant as a whole rather than attempting trimming subsystems. Therefore our model is expressed in Equation 1 as well.

2.2. *Data*

To determine the cost for every location on the moon, a global lunar map of Ilmenite weight ratio is required. In a previous work by Hiroyuki Sato et al. (2017) an almost global TiO2 abundance map was created, where the values of weight percent for TiO2 are used as equivalent for Ilmenite. The resulting map had a mask applied to leave only lunar mare regions and had a limited latitude coverage from 70° S to 70° N. The limited coverage is caused by the sensor method to measure the reflectance of sunlight which is working less reliable with an increasingly steep sunlight angle towards the poles. The initial data was created by the Lunar Reconnaissance Orbiter Camera (LROC) Wide Angle Camera (WAC) which will be our starting point for the creation of our global Ilmenite map. First, the WAC data segments have been joined together resulting in a 27360×10640 resolution of 8-bit encoded values, plotted in Figure 1 below.

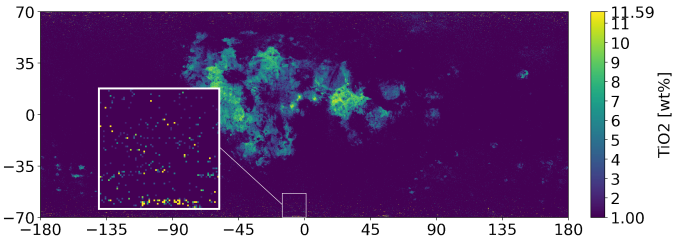

Figure 1: Combined original data from WAC Sato et al. (2017)

One problem are unusual high measurements towards the poles that are considered increasing noise which is scattered through the entire longitudinal axis. The second problem is the incomplete coverage of latitude and therefore the poles itself. To derive an estimation over the missing information at latitudinal coverage, the following strategy was applied. If Ilmenite abundance correlates with the classification of highlands/ mare and the pole regions geology is featuring highland characteristics then the expected value of the known highland region serves as an estimate of Ilmenite content at the poles.

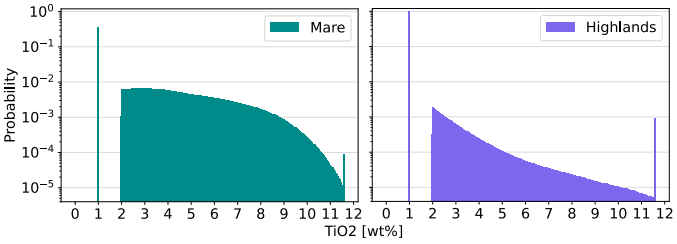

Figure 2: Distribution of Ilmenite content clustered into Highlands and Mare (equirectangular corrected) on combined WAC data with Mare boundaries from Nelson et al. (2014)

As Figure 2 shows, the distribution characteristics of these two regions deviate considerably, whereby the average abundance also differs from 3,38 wt% in Mare to 1,1 wt% in Highland regions. Therefore the Ilmenite content correlation is given and the estimate over the missing latitudinal area is set to 1 wt% as a conservative assumption.

To additionally remove the increasing noise at further extreme latitudes, which start to occur at around ±56 deg, a mask was created out of the mare boundaries merged with a constant separation at ±56 deg latitude displayed in Figure 3.

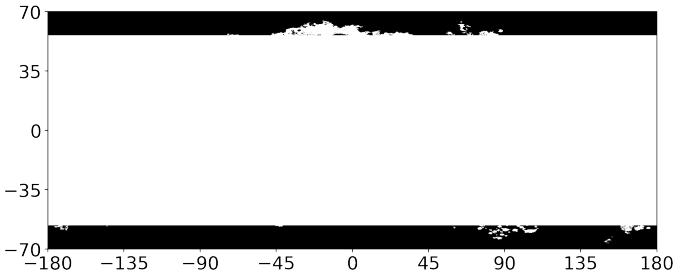

Figure 3: Mask from Mare boundaries from Nelson et al. (2014) and separation at ±56° Latitude (black is set to 1 wt%)

With this mask applied, all values that are not in a Mare region and are outside of ±56 deg are set to 1 wt% while remaining the original values for the rest. Together with the application of the estimates for the polar regions, our global Ilmenite map is completed and can be seen in Figure 4 below.

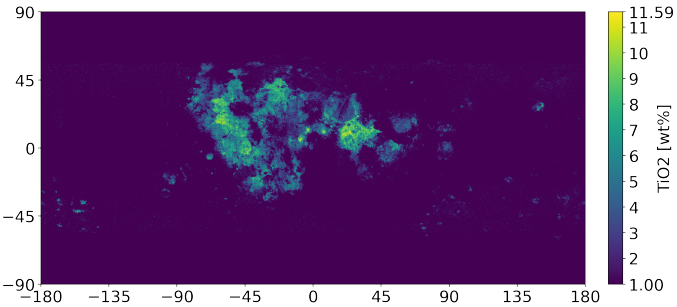

Figure 4: Global Ilmenite map based on WAC and estimates

This global Ilmenite map in Figure 4 is now used as input to our Equation 1, which result is represented in the global cost map in Figure 5.

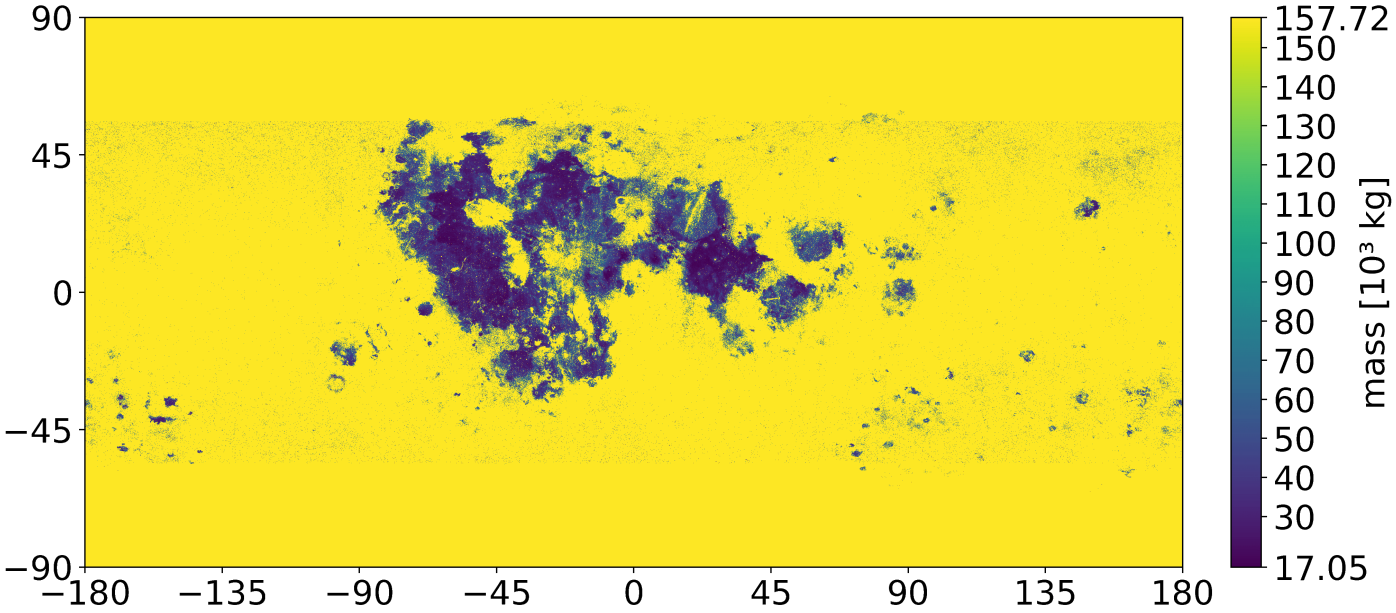

Figure 5: Global cost map for hardware mass by ISRU efficiency

The original resolution from the combined original WAC data was kept and only extended latitudinal resulting in our global Ilmenite map featuring 27360 × 13680, 8-bit values. Where the equations result was computed as 27360 × 13680, 64-bit float and compressed into 27360 × 13680, 16-bit values. This corresponds to a geodetic resolution of around 400 m per pixel at the equator.

2.3. Access of Data

The complete processing steps of this chapter can be found in the Python Notebook "A_ISRU_efficiency.ipynb" along with all resources in full resolution at the papers Git-Repository.

3. Option B - Transport efficiency

3.1. Transport Carrier

3.2. Fuel Depot Location

3.2.1. Destination: Lunar Gateway

3.2.2. Destination: Low Lunar Orbit - Equatorial

3.2.3. Destination: Low Lunar Orbit - Polar

3.2.4. Destination: Lagrange points

3.2.5. Destination: Low Earth Orbit - Starship refuel

4. Joined Model - Relevance Comparison

> Joined model: adding ISRU hardware mass with total used fuel mass of the transport carrier over 10 years.

> Combine pixels into tiles that can be ranked globally. Table showing best location tile for each of the destinations. Expecting all to feature the same location, because ISRU efficiency is more relevant.

> Visualizing composition of combined cost with each portion of spread. Proving transport efficiency not being able to change the ISRU optimal location because its spread has not enough impact.

> Give the amount of years when transport efficiency would become relevant for this scenario.

Appendix A. Mission Settings - AGI Astrogator

Appendix A.1. Destination: Lunar Gateway

Appendix A.2. Destination: Low Lunar Orbit - Equatorial

Appendix A.3. Destination: Low Lunar Orbit - Polar

Appendix A.4. Destination: Lagrange points

Appendix A.5. Destination: Low Earth Orbit - Starship refuel

References

Nelson, D.M., Koeber, S.D., Daud, K., Robinson, M.S., Watters, T.R., Banks, M.E., Williams, N.R., 2014. Mapping lunar maria extents and lobate scarps using lroc image products. Lunar Planet. Sci. 45, 2861.

Sato, H., Robinson, M.S., Lawrence, S.J., Denevi, B.W., Hapke, B., Jolliff, B.L., Hiesinger, H., 2017. Lunar mare tio 2 abundances estimated from uv/vis reflectance. Icarus 296, 216–238. doi:10.1016/j.icarus.2017.06.013.